

The Cost of a Free Lunch: Evidence from U.S. Derivatives Markets

Useong Shin*

April 23, 2026

Abstract

Put–call parity is a terminal-payoff identity; quoted residuals against traded futures are near zero. Yet enforcing parity is path-dependent, exposing arbitrageurs to daily settlement, margin, and finite capital. Using minute-level NBBO data on S&P 500 and Russell 2000 options, I extract option-implied discount factors, compare them with the OIS curve, and construct an annualized *carry gap* (sample median ≈ 37 bp, $>98\%$ positive). A reduced-form specification centered on a volatility $\times\sqrt{\tau}$ path-risk term links the carry gap to implementation risk, trading frictions, and financial conditions, with coefficient signs stable across leave-one-year-out validation. The carry gap is an implementation wedge invisible in price space but systematic in carry space.

JEL: G12; G13; G14;

Keywords: carry gap; put–call parity; spot–future parity; parity violation; path risk; limits to arbitrage

Acknowledgments: I am grateful to Michele Azzone (Politecnico di Milano) for generously sharing OIS data, for guidance on implementing the implied-discount-factor pipeline, and for detailed feedback on earlier drafts; to Baeho Kim (Korea University) for helpful discussions on the theoretical landscape of path-risk pricing and limits to arbitrage; and to Chaehwan Won (Sogang University) for raising critical questions about potential measurement artifacts that helped shape the robustness design of the draft. All remaining errors are my own.

*Sogang Business School, Sogang University (Seoul, Korea).
ORCID: [0009-0003-0197-9003](https://orcid.org/0009-0003-0197-9003)
Email: useong@sogang.ac.kr

1 Introduction

Put–call parity is among the most fundamental no-arbitrage relations. Combining a European call, a put at the same strike and maturity, the underlying, and a risk-free bond locks in a deterministic terminal payoff, so any parity residual should invite immediate arbitrage. Indeed, quoted parity residuals measured against traded futures are tightly compressed around zero, as Figure 1.1 shows.

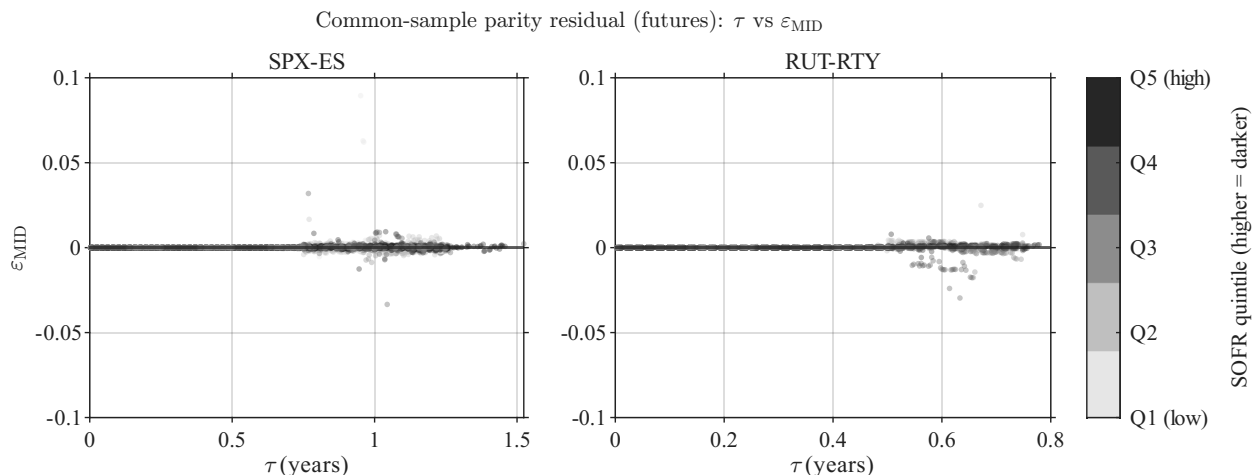


Figure 1.1: Quoted put–call parity residual computed against traded futures-implied forwards. Residuals cluster tightly around zero in both markets.

However, replacing the traded-futures forward with a synthetic forward constructed from the spot index, the OIS curve, and dividend information produces a strikingly different picture. Figure 1.2 shows that even when quoted residuals remain small, systematic residual structure emerges on a carry basis.

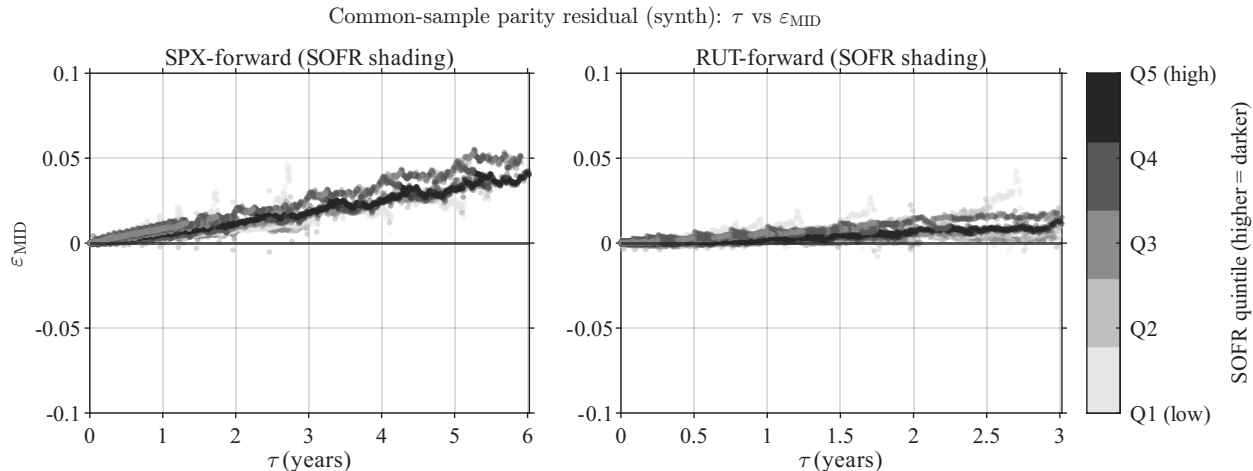


Figure 1.2: Parity residual computed against a synthetic forward constructed from the spot index, OIS curve, and dividend information. Unlike the traded-futures benchmark, a systematic residual structure is visible.

This contrast is the starting point of the paper. Does a small quoted residual imply that enforcing parity is costless and riskless? Answering this question requires separating two propositions. First, put–call parity is an identity over terminal payoffs. Second, the arbitrage trade that enforces this identity is a strategy that must be maintained along a pre-maturity path. The former is a static relation at expiration; the latter is a path-dependent implementation problem exposed to daily settlement, variation margin, funding costs, non-synchronous execution, illiquidity, and finite capital.

A parity-enforcement position may have a deterministic terminal payoff, yet this does not guarantee that the implementation path is risk-free. The trader must absorb interim mark-to-market losses, and an adverse price path can force additional capital injections or involuntary position reduction. Hence, even if visible residuals are compressed by arbitrage activity, the risks and capital commitment embedded in implementation need not vanish with them. This paper focuses precisely on this distinction. I examine whether a systematic wedge attributable to implementation risk and capital constraints can be observed in carry space even when visible price-space residuals converge to near zero.

To this end, I extract option-implied discount factors from minute-level NBBO data on S&P 500 and Russell 2000 options, and construct the carry gap by comparing them with a bootstrapped OIS curve, following the identification approach of [Azzone and Baviera \(2021\)](#).

The results are consistent along three dimensions. First, the carry gap is centered in positive territory in both markets, exhibiting distributional properties difficult to attribute to microstructure noise or measurement error. Second, it retains a pronounced low-frequency structure and regime-dependent persistence even after daily aggregation. Third, these pat-

terns survive a range of robustness checks.

To interpret these empirical facts, I introduce a path-risk term derived from geometric Brownian motion. If parity-enforcement positions are exposed to interim losses and capital-support requirements before maturity, the expected capital commitment scales systematically as a function of volatility and time to maturity. Building on this intuition, I place a volatility $\times\sqrt{\tau}$ path-risk term at the center of the regression specification, supplemented by trading-friction and broad financial-condition variables. The specification exhibits significant in-sample explanatory power, and the signs of all key coefficients remain stable across leave-one-year-out (LOYO) out-of-sample validation.

The contributions of this paper are as follows. First, I explicitly separate the terminal-payoff identity of put–call parity from its implementation as a trading strategy, showing that a small parity residual does not automatically imply risk-free enforcement. Second, I document that the carry gap—defined as the difference between option-implied and OIS-benchmark discount factors, annualized—is a systematic empirical object with a positive center, low-frequency persistence, and state dependence. Third, through a reduced-form specification centered on a path-risk term, I show that implementation risk and capital commitment constitute the core explanatory block of the carry gap. These results suggest that the positive return to parity arbitrage should be understood not as a risk-free “free lunch” but as equilibrium compensation for implementation risk and capital commitment.

The remainder of the paper is organized as follows. Section 2 reviews the related literature. Section 3 describes the data and methodology. Section 4 presents the carry-gap estimates. Section 5 introduces the reduced-form regression specification centered on the path-risk term. Sections 6 and 7 report in-sample estimation results and LOYO out-of-sample validation, respectively. Section 8 presents robustness checks using Treasury constant-maturity yields (DGS) in place of OIS. Section 9 discusses economic implications and limitations, and Section 10 concludes. Additional maturity-bin-level time-series fit results are provided in Appendix A.

2 Related Literature

This paper connects to three strands of the put–call parity literature: the theoretical formulation and empirical testing of the parity relation, the interpretation of observed deviations through market frictions and limits to arbitrage, and the reverse-engineering of option-implied discount rates or funding conditions from parity. I directly build on the empirical strategy of the third strand, extending it with a longer time series and dynamic analysis to recast parity deviations as a dynamic object systematically linked to state variables.

Put–call parity was formally established by [Stoll \(1969\)](#), who already noted that transaction costs, short-sale constraints, and dividend uncertainty could cause the relation to manifest as a no-arbitrage band rather than a point equality. Subsequent early empirical work focused on whether observed deviations constituted genuine arbitrage opportunities or reflections of execution costs ([Gould and Galai, 1974](#); [Klemkosky and Resnick, 1979](#); [Ackert and Tian, 2001](#)). The common conclusion was that deviations should be read as empirical residuals under execution constraints rather than outright failures of no-arbitrage logic. This literature, however, focused on the *existence* of deviations without analyzing the dynamic structure they form over time.

This perspective was generalized in the *limits-to-arbitrage* literature. Following [Shleifer and Vishny \(1997\)](#), a body of work showed that arbitrage is exposed to funding constraints, margin requirements, and path-dependent payoffs, so that theoretical mispricings need not be eliminated instantaneously ([Gromb and Vayanos, 2002](#); [Brunnermeier and Pedersen, 2009](#); [Mitchell and Pulvino, 2012](#)). In derivatives markets, [Ofek et al. \(2004\)](#) documented that parity violations are more frequent and larger for stocks with tighter short-sale constraints. While this literature provides the core economic motivation for the present study, it did not aggregate parity deviations into a daily time series and directly examine their co-movement with financial-condition variables.

Separately, [Brenner and Galai \(1986\)](#) reverse-engineered implied interest rates from option prices and compared them with actual short-term rates, showing that implied rates can vary systematically with maturity. This suggested that parity can serve not only as a no-arbitrage test but also as a tool for inferring market participants’ discount rates and funding conditions.

The most directly related predecessor is [Azzone and Baviera \(2021\)](#). They estimated option-implied discount factors from European put–call parity and, comparing them with the OIS curve, reported an average funding spread of approximately 34 bp in S&P 500 options. I inherit their identification logic and empirical pipeline. Whereas [Azzone and Baviera \(2021\)](#) focused on the static level measurement of implied discount factors, I extend the analysis to a longer time series and a richer panel, placing the time-series structure of the deviation and its dynamic linkage to state variables at the center of the investigation.

In summary, whereas the prior literature has treated parity deviations as (i) empirical tests of no-arbitrage relations, (ii) by-products of market frictions and limited arbitrage, or (iii) static estimates of implied discount rates, this paper asks not whether the deviation exists but what structure it forms over time and why it resists reduction to high-frequency frictions or measurement error.

3 Data and Methodology

3.1 Data and sample scope

I extract market-implied discount factors from SPX and RUT options and compare them with OIS discount factors to measure the carry gap. The identification follows the synthetic-forward procedure proposed by [Azzone and Baviera \(2021\)](#), whose key advantage is that the discount factor implicit in the market can be recovered from European call and put prices at the same maturity alone.

An earlier implementation that combined the spot index, interest-rate curve, and dividend information directly to construct market carry proved sensitive to spot–option nonsynchronicity, dividend estimation error, and arbitrary moneyness selection. The [Azzone and Baviera \(2021\)](#) procedure performs identification entirely within the option cross-section, substantially reducing dependence on exogenous inputs and remaining computationally light enough for repeated analysis across a long sample and a wide maturity spectrum.

Option quotes are minute-level NBBO data collected from ThetaData. Although option data are available through December 31, 2025, the analysis sample is restricted to January 4, 2016 through October 31, 2025 to match the availability of OIS data. All results in the paper are based on the common sample in which option-market information and OIS discount curves are simultaneously observable.

Both SPX and RUT options are European-style index options, so no early-exercise premium arises—a feature that reduces institutional noise in parity-based discount-factor identification.

All empirical analysis is conducted in MATLAB R2025b.¹

3.2 Identification of option-implied discount factors

The identification logic follows [Azzone and Baviera \(2021\)](#). For a European call and put at strike K with maturity T observed at time t , put–call parity can be written as

$$C_t(K, T) - P_t(K, T) = B_t(T)(F_t(T) - K), \quad (1)$$

where $B_t(T)$ is the market-implied discount factor and $F_t(T)$ is the forward value at the same maturity.

¹On 16 parallel workers, the full pipeline for both markets executes in approximately one hour.

Defining the synthetic forward as

$$\mathcal{G}_t(K, T) = C_t(K, T) - P_t(K, T), \quad (2)$$

no-arbitrage requires the forward value to be independent of K , so the market-implied discount factor is identified as the value that makes

$$F_t(T) = \frac{\mathcal{G}_t(K, T)}{B_t(T)} + K \quad (3)$$

constant across strikes.

In practice, for each date–maturity pair I exploit the linear relation between the synthetic forward and the strike to estimate $\hat{B}_t(T)$ and $\hat{F}_t(T)$ simultaneously. The option-implied discount factor is, in effect, the discount rate that eliminates any strike-dependence in the forward price recovered from the synthetic forward.

This identification approach has three advantages. First, it draws on the full strike cross-section within a given maturity, making it less exposed to moneyness selection problems than methods that rely on a specific ATM contract or an arbitrary moneyness range. Second, because $B_t(T)$ and $F_t(T)$ are identified jointly from the strike cross-section, dividends are naturally absorbed into $F_t(T)$, so the dividend estimation problem does not arise directly. Third, the synthetic forward is exactly synchronous with option prices, mitigating the non-synchronicity issues that arise when combining spot, futures, dividend, and interest-rate data separately.

I apply this procedure repeatedly across the full SPX and RUT samples to construct a market×date×maturity panel of implied discount factors.

3.3 OIS curve construction and carry-gap definition

The benchmark discount factor is derived from the OIS curve. Since the financial crisis, OIS has become the standard benchmark for derivatives discounting, and [Azzone and Baviera \(2021\)](#) likewise measured funding spreads against it.

I apply standard bootstrapping to daily OIS data to recover maturity-matched discount factors and zero rates, and construct maturity-matched OIS discount factors for direct comparison with $\hat{B}_t(T)$.

The carry gap is defined as the annualized deviation between the two discount factors. Letting $\tau_t(T) = T - t$,

$$CG_t(T) = \frac{1}{\tau_t(T)} \log \left(\frac{D_t^{\text{OIS}}(T)}{\hat{B}_t(T)} \right), \quad (4)$$

where $D_t^{\text{OIS}}(T)$ is the OIS discount factor and $\hat{B}_t(T)$ is the option-implied discount factor. $CG_t(T) > 0$ indicates that the options market embeds a higher implied carry than the OIS benchmark.

The empirical analysis uses the basis-point-scaled version

$$CG_t^{bp}(T) = 10^4 \cdot CG_t(T), \quad (5)$$

and the daily, market-level carry gap entering regressions is denoted $CG_{i,t}^{bp}$.

3.4 Sample filters and final panel construction

The preprocessing aims to remove observations with excessively low liquidity or unstable price information, thereby ensuring stable cross-sectional identification. Only call–put pairs sharing the same strike and maturity are used. Observations with abnormally low prices or excessive bid–ask spreads are excluded, as are maturities with too few valid strikes for stable cross-sectional identification and dates on which OIS curve recovery fails or the term structure is anomalous. The final sample consists of observations for which (i) the option-implied discount factor can be identified and (ii) the OIS discount factor can be reliably constructed at the same date and maturity.

I construct a date×maturity panel for each of SPX and RUT. Daily time series are aggregated as the median of eligible observations on each date, a procedure that reduces sensitivity to outliers and transient noise while stably tracking the central movement of the carry gap.

4 Carry-Gap Estimates

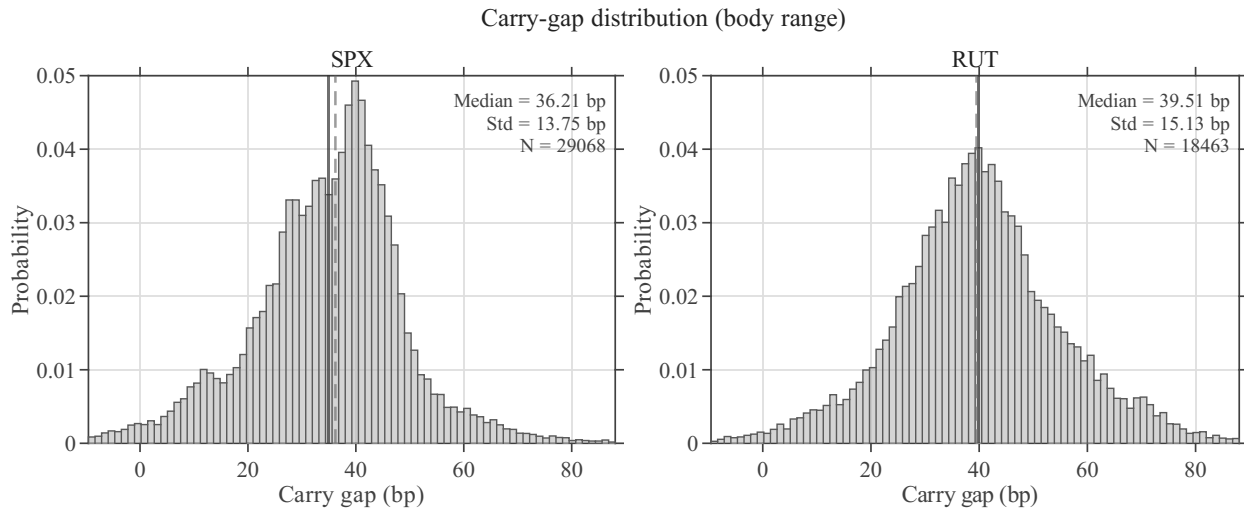


Figure 4.1: Distribution of daily carry gaps for SPX and RUT. Both distributions are centered in positive territory rather than at zero. RUT exhibits a roughly bell-shaped distribution, while SPX displays more pronounced asymmetry.

4.1 Center and cross-market shape

Figure 4.1 shows that the daily carry-gap distribution is distinctly shifted into positive territory in both markets. The full-sample mean is 36.91 bp with a median of 37.50 bp, and 98.4% of observations are positive. By market, the mean and median are 34.87 bp and 36.16 bp for SPX and 40.12 bp and 39.57 bp for RUT. The carry gap is not confined to a single market but constitutes a positive wedge common to both.

The detailed distributional shapes differ across markets. RUT exhibits a relatively smooth bell-shaped distribution, whereas SPX has a sharper peak and a longer right tail. This heterogeneity complements rather than weakens the core finding: the positive center is shared, while the finer shape reflects differences in each market’s liquidity structure and implementation environment.

4.2 Internal consistency and cross-sectional fit

I verify that the positive carry gap is not an artifact of imprecise cross-sectional fitting. The date–maturity-level option cross-sectional regressions in the [Azzone and Baviera \(2021\)](#) pipeline achieve near-perfect fit in both markets. The median cell-level R^2 is 0.9999999 for SPX and 0.9999995 for RUT; the minimum R^2 values are 0.9999972 and 0.9999848,

respectively.²

If the carry gap were merely noise centered at zero, daily aggregation should have driven the distribution’s center toward zero. Instead, the entire distribution is shifted into positive territory and negative observations are exceptional, confirming that the carry gap is a systematic object consistently identified from high-quality option cross-sections.

4.3 Economic magnitude and maturity structure

The full-sample median of approximately 37 bp is broadly comparable to the roughly 34 bp reported by [Azzone and Baviera \(2021\)](#). Because sample composition and measurement details are not identical, direct numerical comparison requires caution, but the consistency with prior work serves as a useful sanity check.

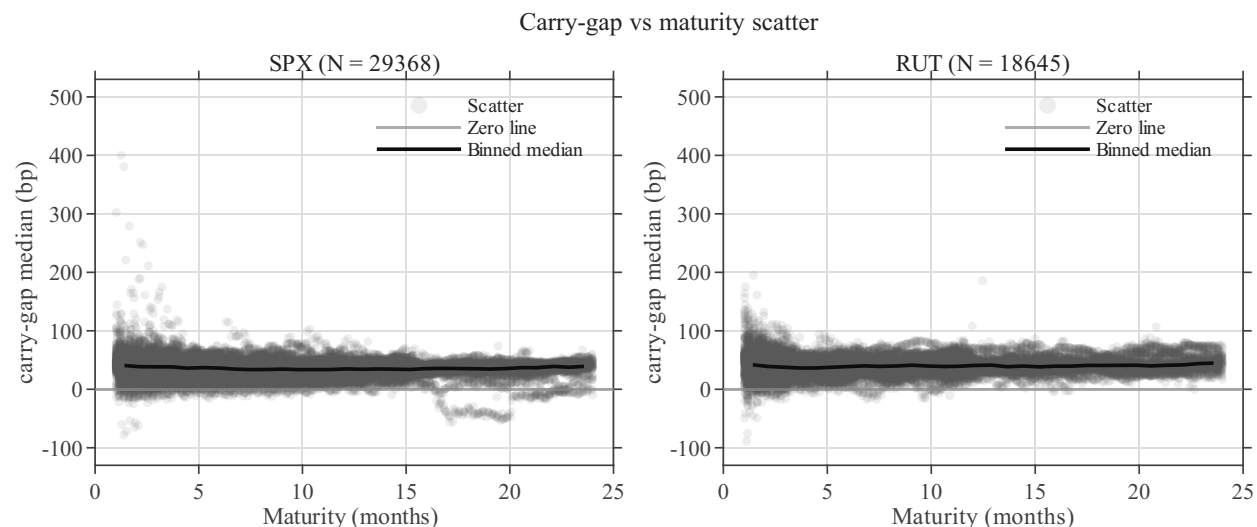


Figure 4.2: Scatter plot of carry gaps against time to maturity. Each point is a date–maturity-level observation; the bold line is the binned median by maturity bucket. Binned medians remain in positive territory across all maturities, while dispersion is markedly wider at the short end.

Figure 4.2 reveals two facts. First, binned medians are stably positive across the entire maturity spectrum, remaining roughly in the 30–40 bp range. The carry gap is not a transient distortion confined to extremely short maturities but a phenomenon that persists across a broad maturity range.

Second, dispersion exhibits strong maturity dependence. In the 1–3 month range, scatter is wide, with outliers exceeding 400 bp, but it compresses rapidly as maturity increases. This

²For some date–maturity combinations, too few observations survive preprocessing for the regression to be estimated. These cases reflect insufficient information for identification rather than poor-quality fits.

reflects a combination of the mechanical amplification from a small τ in the denominator and the economic effect of microstructure frictions—execution nonsynchronicity, illiquidity—weighing more heavily at short horizons.

The finding that the level is flat in maturity while variance is strongly maturity-dependent motivates the need to allow explicit maturity-dependent effects in the regression specification introduced in Section 5.

4.4 Time-series variation

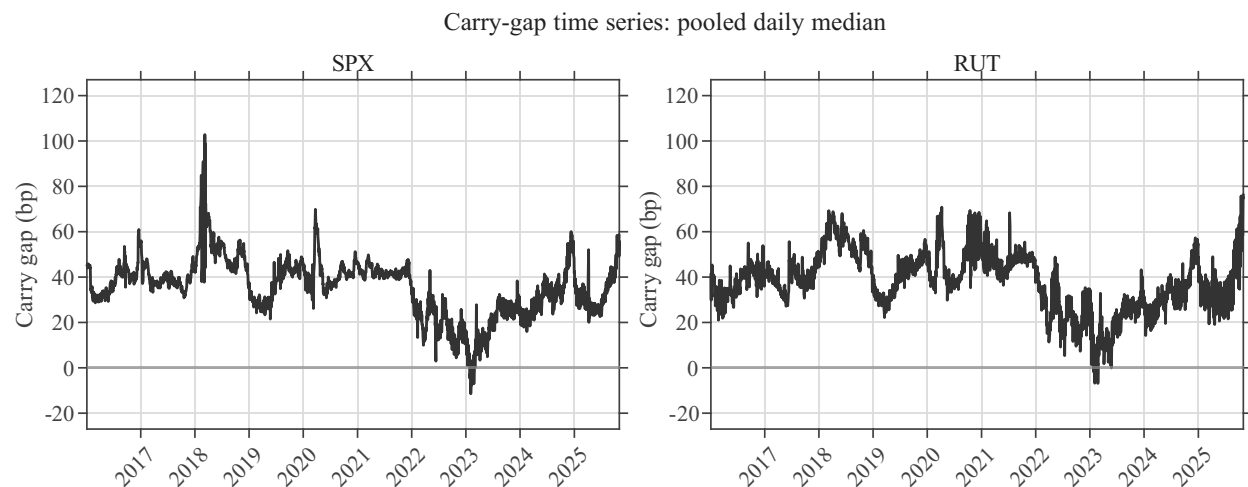


Figure 4.3: Daily carry-gap time series for SPX and RUT. Each value is the pooled daily median across eligible observations on that date. The carry gap remains in positive territory for the majority of the sample and exhibits pronounced level shifts over time.

Figure 4.3 shows that the carry gap is a time-series object with significant level variation. In both markets, it stays in positive territory for the vast majority of the sample and, rather than reverting quickly to zero, undergoes persistent regime-level rises and declines. Meaningful low-frequency structure survives daily aggregation.

Both markets display elevated levels in 2018 and 2020–2021, a decline during 2022–2023, and a rebound in 2024–2025. Although the detailed paths differ across markets, the broad regime shifts are shared, supporting the view that the carry gap contains a systematic component that co-moves with changes in the broader market environment.

In sum, the carry gap exhibits three properties: a positive center, a flat level across maturities, and low-frequency time-series variation. Together, these establish that the carry gap is not mere residual noise but a systematic empirical object observed in carry space.

5 Path-Risk Term and Carry-Gap Regression Specification

This section presents the empirical specification for the carry gap. The key design choice is to introduce the GBM term not as an auxiliary control but as a path-risk term that captures the central structure of the carry gap. Parity is a terminal-payoff identity, yet the trading strategy that enforces it must be maintained along the pre-maturity price path, exposing the trader to daily settlement, variation margin, interim losses, and finite capital constraints. Parity enforcement is therefore better understood as a path-dependent implementation problem than as a static no-arbitrage relation.

This perspective is essential for reconciling two facts simultaneously: quoted parity residuals are very small, yet a systematic wedge can persist in carry space. Even if visible price-space residuals are compressed by arbitrage, the path risk embedded in the implementation process need not vanish automatically. To my knowledge, no prior study has derived the path risk of parity enforcement in an explicit functional form and placed it at the center of a carry-gap regression.

5.1 Intuition and derivation of the path-risk term

The functional form of the GBM term originates from the observation that a parity-enforcement position is exposed to interim mark-to-market losses and capital commitment before maturity. A position combining a synthetic long forward with a short futures contract pays

$$(S_T - K) + (F_0 - S_T) = F_0 - K$$

at maturity and is therefore deterministic at expiration. Before maturity, however, interim futures-price movements alter the margin account, adverse price paths can trigger additional capital requirements, and failure to inject capital promptly jeopardizes position maintenance.

To summarize this in the simplest possible way, let the normalized interim P&L process of the enforcement position be

$$X_t = \sigma B_t,$$

where B_t is a standard Brownian motion and σ is annualized volatility. Under the minimal support rule that prevents the position from insolvency, the cumulative support capital L_t satisfies

$$X_t + L_t \geq 0 \quad \text{for all } t \in [0, T], \quad L_0 = 0$$

and is the smallest nondecreasing process satisfying this constraint:

$$L_t = \sup_{0 \leq s \leq t} (-X_s)^+.$$

By standard properties of Brownian motion, the expected support capital is

$$\mathbb{E}[L_t/N] = \sigma \sqrt{\frac{2t}{\pi}},$$

proportional to volatility and increasing in the square root of time. The average capital commitment over the life of the trade is

$$\bar{B}(T) = \frac{1}{T} \int_0^T \mathbb{E}[L_t/N] dt = \frac{2}{3} \sigma \sqrt{\frac{2T}{\pi}}.$$

Summarizing the opportunity cost of committed capital by a rate-like object r_t , the representative scaling implied by path risk and capital commitment is

$$r_t \bar{B}(T) = r_t \cdot \frac{2}{3} \sigma \sqrt{\frac{2T}{\pi}}.$$

The GBM term used in this paper translates this structure into basis points.

Specifically, for market $i \in \{\text{SPX}, \text{RUT}\}$,

$$GBM_{i,t}^{OIS,xY} = 10^4 \cdot \frac{OISxY_t}{100} \cdot \frac{2}{3} \cdot \frac{Vol_{i,t}}{100} \cdot \sqrt{\frac{2\tau_{i,t}}{\pi}}, \quad x \in \{1, 10\},$$

$$Vol_{i,t} = \begin{cases} VIX_t, & i = \text{SPX}, \\ RVX_t, & i = \text{RUT}. \end{cases} \tag{6}$$

The $x = 1$ component proxies for short-to-medium-term funding conditions, while $x = 10$ proxies for the long-run opportunity cost of capital. The goal is not to estimate this expression as a structural model but to embed the core functional form implied by path-dependent implementation into the empirical specification.

5.2 Baseline specification: pooled regression

The baseline is a pooled regression combining both markets. Its purpose is to identify the average structure of the GBM term common to SPX and RUT and to separate mean-level differences via a market dummy. The estimation sample is restricted to observations with

at least one month to maturity.

$$CG_{i,t}^{bp} = \alpha + \delta D_i^{\text{SPX}} + \phi_1 GBM_{i,t}^{\text{OIS},1Y} + \phi_{10} GBM_{i,t}^{\text{OIS},10Y} + \beta \frac{BA_{i,t}^{\text{med}}}{\tau_{i,t}} + \gamma NFCI_t + \varepsilon_{i,t}, \quad (7)$$

where

$$D_i^{\text{SPX}} = \begin{cases} 1, & i = \text{SPX}, \\ 0, & i = \text{RUT}. \end{cases}$$

$GBM_{i,t}^{\text{OIS},1Y}$ and $GBM_{i,t}^{\text{OIS},10Y}$ are the core explanatory block capturing the central structure of the carry gap, while $BA_{i,t}^{\text{med}}/\tau_{i,t}$ and $NFCI_t$ supplement residual variation left unexplained by the path-risk term.

The GBM coefficients are not fixed at unity because parity enforcement operates in both directions. The $+C - P - F$ and $-C + P + F$ trades share the same path-risk term but carry opposite economic signs. The observed carry gap therefore approximates a net directional imbalance between opposing arbitrage pressures, and the GBM coefficients are naturally interpreted as reduced-form loadings of net directional enforcement pressure on the common term.

5.3 Market-specific specification

Because SPX and RUT differ in liquidity structure, investor base, and microstructure environment, I also estimate market-specific regressions. For each $i \in \{\text{SPX}, \text{RUT}\}$,

$$CG_{i,t}^{bp} = \alpha_i + \phi_{1,i} GBM_{i,t}^{\text{OIS},1Y} + \phi_{10,i} GBM_{i,t}^{\text{OIS},10Y} + \beta_i \frac{BA_{i,t}^{\text{med}}}{\tau_{i,t}} + \gamma_i NFCI_t + \varepsilon_{i,t}. \quad (8)$$

The pooled regression serves as the baseline for confirming common structure, while the market-specific regressions reveal finer heterogeneity on top of it.

5.4 Economic interpretation of regressors

$GBM_{i,t}^{\text{OIS},1Y}$ and $GBM_{i,t}^{\text{OIS},10Y}$ are path-risk terms derived from the path dependence of parity enforcement. They summarize implementation risk scaled by short-to-medium-term funding conditions and long-run capital opportunity cost, respectively. The empirical coefficients measure the magnitude of net directional enforcement pressure across the market.

$BA_{i,t}^{\text{med}}/\tau_{i,t}$ is a trading-friction term based on the median ATM bid–ask spread, summarizing execution cost, execution risk, and the tightness of market-making conditions. It is

constructed so that a given bid–ask level maps more heavily into the annualized carry gap at shorter maturities.

$NFCI_t$ is the Chicago Fed National Financial Conditions Index, proxying for system-wide funding stress and financial tightening that individual option-market indicators alone cannot capture.

D_i^{SPX} is a market dummy that separates the mean-level difference between SPX and RUT while maintaining a common slope structure.

In sum, the specification first explains the carry gap through the GBM path-risk term and then supplements residual variation with trading frictions and financial conditions. The GBM terms are not auxiliary controls but the core block capturing the central empirical structure of the carry gap.

6 In-Sample Results

This section examines the in-sample explanatory power of the GBM-based reduced-form specification. The evaluation focuses not on precise replication of individual observations but on overall fit, consistency of coefficient signs, and the extent to which the specification stably summarizes the structure of the carry gap.

I compare three specifications: a pooled common-market specification with common slope coefficients and an SPX dummy for level differences, and separate specifications for SPX and RUT.

Table 6.1: In-sample fit summary

Specification	Obs.	Trading days	R^2	Adj. R^2	RMSE (bp)	MAE (bp)
Pooled common + SPX dummy	48,013	2,456	0.309	0.309	13.57	9.26
SPX separate	29,368	2,456	0.312	0.312	13.20	8.68
RUT separate	18,645	2,455	0.281	0.281	13.95	10.10

Table 6.2: In-sample coefficient estimates

Regressor	Pooled common + SPX dummy	SPX separate	RUT separate
Intercept	24.901*** (1.427)	23.134*** (1.431)	24.577*** (1.375)
SPX dummy	-0.985*** (0.297)	—	—
$GBM^{OIS,1Y}$	-0.557*** (0.036)	-0.548*** (0.042)	-0.555*** (0.033)
$GBM^{OIS,10Y}$	0.469*** (0.038)	0.411*** (0.044)	0.541*** (0.037)
BA^{med}/τ	0.158*** (0.013)	0.256*** (0.021)	0.130*** (0.012)
$NFCI$	-24.598*** (2.458)	-25.839*** (2.539)	-23.961*** (2.492)

Notes: Standard errors clustered by date are in parentheses. ***, **, * denote significance at the 1%, 5%, and 10% levels, respectively.

6.1 Overall fit

Table 6.1 reports an R^2 of 0.309 and an RMSE of 13.57 bp for the pooled specification. The separate specifications yield R^2 values of 0.312 for SPX and 0.281 for RUT—no dramatic improvement over the pooled baseline. This suggests that the central structure of the carry gap is largely common to both markets.

6.2 Pooled specification

The most important result in Table 6.2 is the sign structure of the GBM block. $GBM^{OIS,1Y}$ enters with a negative sign and $GBM^{OIS,10Y}$ with a positive sign, both strongly significant. The path-risk terms scaled by short-to-medium-term funding conditions and long-run capital opportunity cost load onto the carry gap in opposite directions.

This result is consistent with the interpretation that the carry gap approximates a net directional imbalance between opposing arbitrage pressures rather than the total path cost of one-sided enforcement. The two GBM coefficients can be read as reduced-form loadings of net directional exposure on each rate-like component.

BA^{med}/τ is positive and strongly significant, indicating that wider trading frictions are associated with a larger carry gap. $NFCI$ is negative and strongly significant, indicating a systematic link between the carry gap and broad financial conditions.

The SPX dummy is negative and significant but small in magnitude (approximately 1 bp),

suggesting that cross-market differences manifest more in sensitivity to individual regressors than in mean levels.

6.3 Market-specific specifications

The separate regressions confirm that the core patterns of the pooled specification are stable across markets. The coefficient on $GBM^{OIS,1Y}$ is -0.548 for SPX and -0.555 for RUT—nearly identical—and NFCI is negative with similar magnitude in both markets. The short-to-medium-term GBM term and the financial-conditions block are close to market-common structures.

Cross-market heterogeneity appears primarily in $GBM^{OIS,10Y}$ and BA^{med}/τ . $GBM^{OIS,10Y}$ loads at 0.411 for SPX versus 0.541 for RUT, indicating that RUT responds more strongly to the long-run opportunity-cost channel. BA^{med}/τ loads at 0.256 for SPX versus 0.130 for RUT, indicating that the bid–ask signal translates more forcefully into the carry gap in SPX. The role of the separate regressions is not to negate common structure but to show that sensitivities to the long-run path-risk channel and the trading-friction channel can vary across markets.

6.4 Maturity-bin fit

Explanatory power is higher at intermediate maturities than at the short end. For SPX under the pooled specification, R^2 rises from 0.080 at 1–2 months to 0.530 at 10–14 months, then declines to 0.254 beyond 21 months. A similar pattern holds for RUT, with R^2 reaching 0.440 at 10–14 months and 0.451 at 14–21 months, remaining at 0.363 beyond 21 months.

The separate specifications offer modest improvements in some bins, but the gains are limited. The maturity-bin results reaffirm that the specification’s primary achievement lies in reproducing a common path-risk structure rather than delivering fully customized market-level fits.

6.5 Error diagnostics

The daily mean relative error under the pooled specification is approximately -13% , with a mean absolute relative error of approximately 29% . The separate specifications are similar. All three specifications tend to estimate fitted values slightly conservatively relative to actuals, consistent with the view that this specification is a reduced-form summary of central levels and major regime shifts rather than a model designed to replicate every fine-grained fluctuation.

In sum, the in-sample results support the interpretation that the GBM path-risk term captures the central structure of the carry gap. $GBM^{OIS,1Y}$ and $GBM^{OIS,10Y}$ operate as strong regressors with opposite signs, and the pooled specification’s explanatory power is not materially inferior to the separate specifications. Cross-market heterogeneity exists in the long-run GBM term and the bid–ask term, but the core structure is common across both markets.

7 Out-of-Sample Validation

This section evaluates the out-of-sample performance of the common-market and separate specifications using a leave-one-year-out (LOYO) procedure. Each calendar year is held out in turn, the coefficients are estimated on the remaining years, and fit and coefficient stability are assessed on the held-out year. Two criteria guide the evaluation: how much fit varies across sample splits, and whether coefficient signs collapse randomly year by year or deteriorate only during specific regime transitions.

7.1 LOYO design and evaluation criteria

The LOYO approach reveals sensitivity to year-level regime changes more directly than a single holdout split. The sample spans the pandemic shock, a rapid rate-hiking cycle, and the subsequent stabilization, making it well suited for a regime-sensitivity check.

I use year-level out-of-sample R^2 as the primary metric, interpreted alongside the mean R^2 , median R^2 , pooled R^2 , number of years with positive R^2 , correlation, and RMSE. Sign stability of re-estimated coefficients is examined separately.

7.2 Results

Table 7.1: LOYO out-of-sample performance summary

Specification	Market	Mean R^2	Median R^2	Pooled R^2	Years with $R^2 > 0$	Mean corr.	Mean RMSE (bp)
Common-market	SPX	0.049	0.187	0.212	9/10	0.189	13.93
Common-market	RUT	0.065	0.063	0.173	6/10	0.252	15.16
Separate	SPX	0.059	0.130	0.221	7/10	0.205	13.95
Separate	RUT	0.075	0.108	0.171	6/10	0.243	15.07

Table 7.1 shows that mean R^2 values—0.049 and 0.065 for SPX and RUT under the common-market specification, 0.059 and 0.075 under the separate specification—are modest and do not suggest a strong forecasting model.

However, this weak average performance is not uniformly distributed across years. Positive R^2 is recorded in 9 of 10 years for SPX and 6 of 10 for RUT under the common-market specification, and the median and pooled R^2 are more favorable than the mean. The out-of-sample fit does not fail across the board.

Fit deterioration is concentrated in a small number of holdout years. For SPX, 2020 stands out (R^2 : -1.634 common-market, -1.221 separate). For RUT, 2020 and the 2016–2017 holdouts also produce negative R^2 . By contrast, 2021–2023 delivers solid performance across all four specifications (e.g., 2023 SPX common-market 0.561, RUT common-market 0.664).

Table 7.2: LOYO out-of-sample performance excluding the 2020 holdout

Specification	Market	Mean R^2	Median R^2	Years with $R^2 > 0$	Mean corr.	Mean RMSE (bp)
Common-market	SPX	0.236	0.215	9/9	0.250	13.25
Common-market	RUT	0.119	0.091	6/9	0.263	14.49
Separate	SPX	0.201	0.185	7/9	0.261	13.45
Separate	RUT	0.148	0.153	6/9	0.258	14.26

Table 7.2 confirms this. Excluding 2020, mean R^2 rises to 0.236 (SPX common-market), 0.201 (SPX separate), 0.119 (RUT common-market), and 0.148 (RUT separate). The weakness of the LOYO performance is driven less by structural collapse than by the extreme 2020 regime and a few early RUT holdout years.

Correlations are more favorable than R^2 . Excluding 2020, mean correlations are in the 0.24–0.26 range across all four specifications, suggesting that the regression tracks the direction and regime shifts of the carry gap even when level calibration is unstable. For instance, the SPX 2024 holdout yields R^2 of 0.032 or -0.016 but correlations of 0.618 and 0.589, a case where the time-series shape is tracked but the level calibration is misaligned.

RMSE is approximately 14 bp for SPX and 15 bp for RUT, stabilizing at 13.3–13.5 bp and 14.3–14.5 bp when 2020 is excluded. The specification’s weakness lies not in loss of directionality but in level-calibration failure during specific regimes.

Table 7.3: Sign stability of LOYO re-estimated coefficients

Regressor	Common-market	SPX separate	RUT separate
Intercept	+ 10/10	+ 10/10	+ 10/10
SPX dummy	- 10/10	—	—
$GBM^{OIS,1Y}$	- 10/10	- 10/10	- 10/10
$GBM^{OIS,10Y}$	+ 10/10	+ 10/10	+ 10/10
BA^{med}/τ	+ 10/10	+ 10/10	+ 10/10
$NFCI$	- 10/10	- 10/10	- 10/10

Table 7.3 shows that the signs of all key coefficients are perfectly stable. Across all three specifications, $GBM^{OIS,1Y}$ and $NFCI$ are negative in 10 out of 10 holdout years, while $GBM^{OIS,10Y}$ and BA^{med}/τ are positive in 10 out of 10. The instability in out-of-sample fit does not stem from random sign collapse but from joint variation in coefficient magnitudes and level calibration during specific shock episodes.

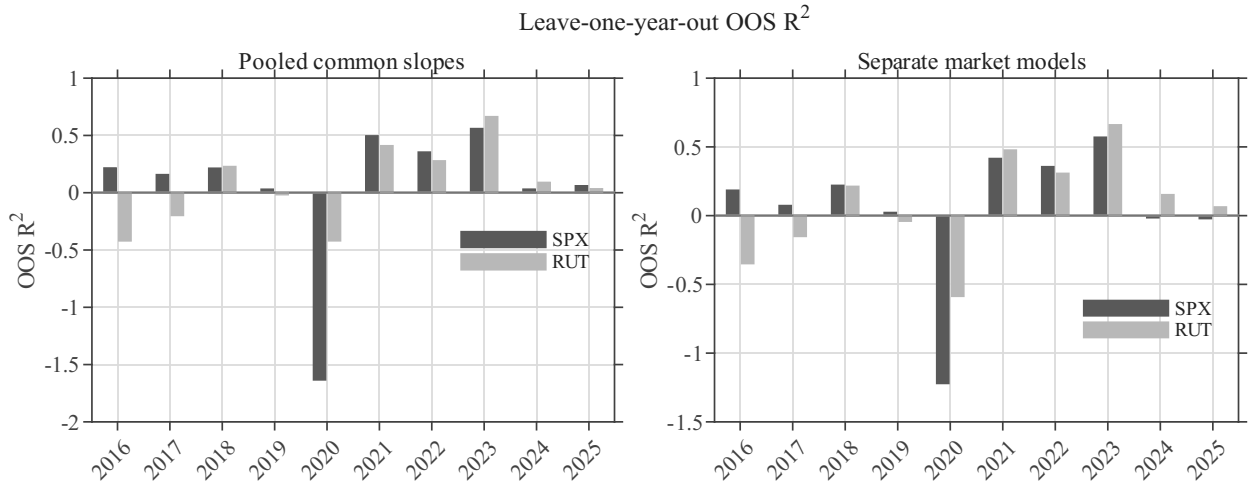


Figure 7.1: Year-level LOYO out-of-sample R^2 for the common-market and separate specifications. Most holdout years produce positive or near-zero R^2 , but the 2020 holdout for SPX and a few early holdout years for RUT generate sharply negative values that drag down the overall mean.

7.2.1 Common-market specification

The common-market specification imposes a common coefficient structure and therefore constitutes the most conservative out-of-sample test. Even so, positive R^2 obtains in 9/10 years for SPX and 6/10 for RUT, and excluding 2020 raises mean R^2 to 0.236 (SPX) and 0.119 (RUT). Sign stability is perfect. A common structure exists, but level calibration may lack sufficient flexibility during abrupt regime transitions such as the pandemic.

7.2.2 Separate specifications

The separate specifications allow market-level heterogeneity, but the actual improvement is modest. Mean R^2 is 0.059 (SPX) and 0.075 (RUT), similar to the common-market results; pooled R^2 is 0.221 (SPX) and 0.171 (RUT).

The advantage of the separate specifications lies not in a dramatic R^2 gain but in naturally accommodating market-specific coefficient structures. Under LOYO, the signs of all four key variables are preserved across all 10 holdout years, confirming that the in-sample patterns are not artifacts of any particular year.

In sum, the LOYO results indicate that this specification is not a strong forecasting model but a reduced-form structure that falters during regime transitions yet works repeatedly in normal regimes. The concentration of fit deterioration in a few holdout years and the perfect sign stability of all key coefficients suggest that the specification captures a regime-dependent economic structure rather than being a product of overfitting.

8 Robustness: DGS as an Alternative Benchmark

This section reports robustness checks in which the discount benchmark is replaced by Treasury constant-maturity yields (DGS) instead of OIS. The sample period is kept identical—January 4, 2016 through October 31, 2025—to permit direct comparison with the OIS baseline. Two questions are addressed. First, does the core structure centered on the GBM path-risk term survive under DGS? Second, if so, which coefficients are robust and which are sensitive to benchmark choice?

8.1 In-sample results

Table 8.1: In-sample fit summary under the DGS benchmark

Specification	Obs.	Trading days	R^2	Adj. R^2	RMSE (bp)	MAE (bp)
Common-market + SPX dummy	48,030	2,457	0.229	0.229	14.96	10.56
SPX separate	29,377	2,457	0.234	0.234	14.36	9.85
RUT separate	18,653	2,456	0.208	0.208	15.66	11.60

Table 8.1 shows that explanatory power weakens relative to the OIS baseline (common-market R^2 : OIS 0.309 \rightarrow DGS 0.229), though results do not collapse entirely and the relative structure between common-market and separate specifications is largely preserved.

The most important finding in the coefficient estimates is that the sign structure of the dual GBM term is maintained. $GBM^{DGS,1Y}$ is negative and $GBM^{DGS,10Y}$ is positive across all three specifications, both strongly significant. BA^{med}/τ remains positive and NFCI remains negative, preserving the same directional pattern as the OIS baseline.

However, the coefficient on $GBM^{DGS,10Y}$ is smaller in magnitude than under OIS, and the absolute value of the NFCI coefficient also shrinks. Maturity-bin-level fit deteriorates notably at longer horizons: for SPX under the common-market specification, R^2 is 0.176 at 10–14 months and -0.111 beyond 21 months. In summary, the DGS in-sample results preserve the core sign structure but deliver weaker term-structure fit at the long end relative to OIS.

8.2 Out-of-sample results

Table 8.2: LOYO out-of-sample performance summary under the DGS benchmark

Specification	Market	Mean R^2	Median R^2	Pooled R^2	Years with $R^2 > 0$	Mean corr.	Mean RMSE (bp)
Common-market	SPX	0.053	0.192	0.170	7/10	0.213	15.05
Common-market	RUT	0.036	0.169	0.121	6/10	0.201	16.90
Separate	SPX	-0.039	0.237	0.141	7/10	0.236	15.31
Separate	RUT	0.065	0.148	0.145	7/10	0.190	16.73

Table 8.2 shows that mean R^2 values are generally weak, with SPX separate recording a negative mean R^2 . However, median and pooled R^2 are positive throughout, and 6–7 out of 10 years produce positive R^2 , so the specification does not fail uniformly.

Fit deterioration is concentrated in specific regime-transition periods. Under OIS, 2020 was the most vulnerable holdout; under DGS, 2022 is more prominent (SPX common-market $R^2 = -1.167$, separate -1.352). Even excluding 2020, mean R^2 remains modest—SPX common-market 0.108, separate 0.111; RUT common-market 0.073, separate 0.072—because the large negative contribution from 2022 persists. The DGS out-of-sample results are thus sensitive not only to the pandemic shock but also to abrupt changes in the rate environment.

Table 8.3: Sign stability of LOYO re-estimated coefficients under the DGS benchmark

Regressor	Common-market	SPX separate	RUT separate
$GBM^{DGS,1Y}$	– 10/10	– 10/10	– 10/10
$GBM^{DGS,10Y}$	+ 10/10	+ 10/10	+ 10/10
BA^{med}/τ	+ 10/10	+ 10/10	+ 10/10
NFCI	– 10/10	– 10/10	– 10/10
SPX dummy	mixed (+ 1/10, – 9/10)	—	—

Table 8.3 shows that the signs of all core coefficients remain highly stable under DGS. $GBM^{DGS,1Y}$ is negative in 10/10 holdout years, $GBM^{DGS,10Y}$ and BA^{med}/τ are positive in 10/10, and NFCI is negative in 10/10. Only the SPX dummy flips to positive in the 2020 holdout, with no impact on the stability of the core block.

Overall, the DGS robustness check does not erase the paper’s central message. The sign structure of the dual GBM term remains stable both in-sample and out-of-sample, indicating that the core results are not artifacts of a particular discount benchmark. Quantitative performance is, however, weaker than under OIS, especially in long-maturity-bin fit and out-of-sample performance during rate-regime transitions. The DGS results therefore confirm the robustness of the basic findings while supporting the view that OIS provides the empirically more stable baseline.

9 Discussion

This section organizes the implications of the empirical results along five dimensions.

9.1 Empirical performance of the GBM path-risk term

The central empirical finding is that GBM^{1Y} and GBM^{10Y} are repeatedly significant with opposite signs and different magnitudes. The carry gap is not a simple discount-rate level effect or measurement error but is organized in a manner consistent with the path-risk structure of parity enforcement.

The opposite signs can be interpreted through the lens of the term structure of arbitrage capital. The negative coefficient on $GBM^{OIS,1Y}$ reflects asymmetric transmission of the short-end discount structure. When short-term rates rise, the OIS discount factor D^{OIS} falls immediately, but the option-implied discount factor \hat{B} , identified within the option cross-section, may not respond at the same speed. As a result, the carry gap $\log(D^{OIS}/\hat{B})$ is mechanically compressed when short rates rise, and this effect, amplified by volatility $\times\sqrt{\tau}$, manifests as a negative sensitivity to $GBM^{OIS,1Y}$.

The positive coefficient on $GBM^{OIS,10Y}$, by contrast, reflects a long-run capital opportunity-cost channel. A higher 10-year risk-free yield raises the opportunity cost of committing capital to parity enforcement. Following the capital-allocation logic of Shleifer and Vishny (1997) and Brunnermeier and Pedersen (2009), finite arbitrage capital migrates elsewhere when outside opportunities improve, reducing the capital available for parity enforcement and widening the equilibrium carry gap.

I do not structurally separate these two channels, but the observed sign pattern is con-

sistent with this interpretation, and the 10/10 sign stability under LOYO supports the view that the structure is not a sample-specific accident.

To be clear, “systematic” here does not mean that the carry gap can be precisely forecasted. Mean LOYO R^2 is modest and fit varies across regimes. The systematicity I emphasize lies in the directionality and repeatability of the economic relations that organize the carry gap.

9.2 Common structure and cross-market heterogeneity

SPX and RUT are neither fully distinct nor fully identical. Both markets exhibit a positive center, low-frequency persistence, and structural links to the GBM term, trading frictions, and financial conditions, and the pooled specification’s fit is not materially inferior to the separate regressions.

Cross-market heterogeneity appears primarily in GBM^{10Y} and BA^{med}/τ . Sensitivity to GBM^{10Y} is larger in RUT, while sensitivity to BA^{med}/τ is larger in SPX. GBM^{1Y} and NFCI, by contrast, are stably repeated across markets. SPX and RUT are best understood as two markets sharing a common path-risk structure onto which certain channel intensities are layered differently.

9.3 Commonalities and differences between OIS and DGS

The core sign structure survives under DGS: GBM^{1Y} negative, GBM^{10Y} positive, BA^{med}/τ positive, NFCI negative—a result that does not depend on benchmark choice.

The two benchmarks are not interchangeable, however. OIS delivers more stable in-sample fit and better long-maturity term-structure performance, while DGS is more vulnerable to the 2022 rate-regime transition. Considering coefficient structure and interpretive stability together, OIS is the more natural reference point. The DGS results are best read as a robustness check confirming that the GBM term operates robustly while its quantitative strength can vary with benchmark choice.

9.4 Economic meaning of parity enforcement and the carry gap

Put–call parity is exact as a terminal-payoff identity, and quoted residuals in price space are very small. Yet converting the same data into carry reveals a systematic object with a positive center, low-frequency persistence, and state-variable dependence whose central structure aligns with the GBM path-risk term. Whether a parity relation “holds” and at what cost and risk it is “enforced” are distinct questions.

Parity enforcement must be maintained along the pre-maturity path, subject to daily settlement, variation margin, capital commitment, and execution nonsynchronicity. These burdens may be invisible in price space yet persist as a systematic positive wedge in carry space. The positive return to parity arbitrage is more plausibly interpreted as compensation for implementation risk and capital commitment than as a risk-free profit.

9.5 Unexplained component at the short end

Explanatory power at the 1–2 month horizon is markedly lower than at intermediate maturities. This does not negate the GBM term but suggests that a separate residual component remains at the short end. In pilot tests, an ad hoc correction term amplifying the short-maturity contribution of the GBM term yielded limited improvement, suggesting that the issue may involve a distinct short-end component rather than shape misspecification of the existing term. Beyond documenting the central structure of the carry gap, a contribution of this paper is to reveal the possible existence of a short-end-specific component not captured by the current specification.

9.6 Limitations and future work

First, this study is a reduced-form analysis. The coefficients reflect conditional associations, not structural causal effects. Building a structural model in which implementation risk and capital constraints endogenously generate an equilibrium wedge is left for future work.

Second, the choice of discount benchmark is itself an economic question. Exploring reference points that more directly reflect market participants' actual funding costs or capital opportunity costs is a worthwhile extension.

Third, the sample is limited to two U.S. equity-index option markets. Comparing results with European or Asian index options or other underlying assets would clarify the generality of the observed structure.

Fourth, while LOYO coefficient signs are stable, out-of-sample fit varies across regimes. Using more granular microdata to directly identify the links between execution risk, margin burdens, market-maker capital constraints, and the carry gap could help isolate the sources of this regime dependence.

10 Conclusion

This paper separates two propositions about put–call parity: the terminal-payoff identity itself, and the stronger claim that enforcing it in practice is economically risk-free. The

former is exact; the latter does not follow automatically once daily settlement, variation margin, capital commitment, and liquidation risk under finite capital are taken into account.

The empirical evidence from U.S. equity-index option markets shows that this distinction manifests not in price space but in carry space. Quoted parity residuals are compressed near zero, yet annualizing the gap between option-implied and benchmark discount structures reveals a systematic carry gap with a positive center, low-frequency persistence, and state-variable dependence. The GBM path-risk term introduced in this paper operates as the central explanatory block of this carry gap: its two components, scaled by short-to-medium-term and long-term interest rates, are repeatedly significant with opposite signs and different magnitudes. The signs of all key coefficients are stable under LOYO out-of-sample validation and survive replacement of the discount benchmark with DGS.

The carry gap is an empirical object showing that the economic burden of parity enforcement persists even in markets where visible parity residuals have nearly vanished. As long as parity enforcement remains a path-dependent, capital-intensive activity, markets may nearly eliminate visible price-space residuals without fully closing the wedge in carry space. The GBM path-risk term offers a viable starting point for interpreting the structure of that wedge.

Funding

This research did not receive any specific grant from funding agencies in the public, commercial, or not-for-profit sectors.

Declaration of AI usage in manuscript preparation

During the preparation of this manuscript, the author used ChatGPT (OpenAI) and Claude (Anthropic) for language refinement and structural clarity. All outputs were reviewed and edited by the author, who takes full responsibility for the content.

Declaration of interest

The author declares no competing interests.

References

- Stoll, H. R. (1969). The Relationship between Put and Call Option Prices. *The Journal of Finance*, 24(5), 801–824. <https://doi.org/10.1111/j.1540-6261.1969.tb01694.x>
- Gould, J. P., & Galai, D. (1974). Transaction Costs and the Relationship between Put and Call Prices. *Journal of Financial Economics*, 1(2), 105–129. [https://doi.org/10.1016/0304-405X\(74\)90001-4](https://doi.org/10.1016/0304-405X(74)90001-4)
- Klemkosky, R. C., & Resnick, B. G. (1979). Put–Call Parity and Market Efficiency. *The Journal of Finance*, 34(5), 1141–1155. <https://doi.org/10.1111/j.1540-6261.1979.tb00061.x>
- Brenner, M., & Galai, D. (1986). Implied Interest Rates. *The Journal of Business*, 59(3), 493–507. <https://doi.org/10.1086/296349>
- Shleifer, A., & Vishny, R. W. (1997). The Limits of Arbitrage. *The Journal of Finance*, 52(1), 35–55. <https://doi.org/10.1111/j.1540-6261.1997.tb03807.x>
- Ackert, L. F., & Tian, Y. S. (2001). Efficiency in Index Options Markets and Trading in Stock Baskets. *Journal of Banking & Finance*, 25(9), 1607–1634. [https://doi.org/10.1016/S0378-4266\(00\)00145-X](https://doi.org/10.1016/S0378-4266(00)00145-X)
- Gromb, D., & Vayanos, D. (2002). Equilibrium and Welfare in Markets with Financially Constrained Arbitrageurs. *Journal of Financial Economics*, 66(2–3), 361–407. [https://doi.org/10.1016/S0304-405X\(02\)00228-3](https://doi.org/10.1016/S0304-405X(02)00228-3)
- Ofek, E., Richardson, M., & Whitelaw, R. F. (2004). Limited arbitrage and short sales restrictions: evidence from the options markets. *Journal of Financial Economics*, 74(2), 305–342. <https://doi.org/10.1016/j.jfineco.2003.05.008>
- Brunnermeier, M. K., & Pedersen, L. H. (2009). Market Liquidity and Funding Liquidity. *The Review of Financial Studies*, 22(6), 2201–2238. <https://doi.org/10.1093/rfs/hhn098>
- Mitchell, M., & Pulvino, T. (2012). Arbitrage Crashes and the Speed of Capital. *Journal of Financial Economics*, 104(3), 469–490. <https://doi.org/10.1016/j.jfineco.2011.09.002>
- Azzone, M., & Baviera, R. (2021). Synthetic Forwards and Cost of Funding in the Equity Derivative Market. *Finance Research Letters*, 41, 101841. <https://doi.org/10.1016/j.fr1.2020.101841>

Board of Governors of the Federal Reserve System (US) (2026a). Federal Reserve Bank of Chicago, Chicago Fed National Financial Conditions Index [NFCI], retrieved from FRED, Federal Reserve Bank of St. Louis, April 3, 2026. <https://fred.stlouisfed.org/series/NFCI>.

Board of Governors of the Federal Reserve System (US) (2026b). Federal Reserve Bank of New York, Market Yield on U.S. Treasury Securities at 10-Year Constant Maturity, Quoted on an Investment Basis [DGS1MO, DGS3MO, DGS6MO, DGS1, DGS2, DGS3, DGS5, DGS7, DGS10], retrieved from FRED, Federal Reserve Bank of St. Louis, April 3, 2026. <https://fred.stlouisfed.org/series/DGS10>.

A Time-Series Fit by Maturity Bin

This appendix reports the time-series fit of the regression specification presented in Section 6 across individual maturity bins. The main text shows only the representative 10–14 month bin; the full maturity spectrum is provided here to give a more complete picture of the maturity-dependent fit of the carry gap. In each figure, the solid line is the actual daily carry gap and the gray line is the regression fitted value.

A.1 Pooled specification

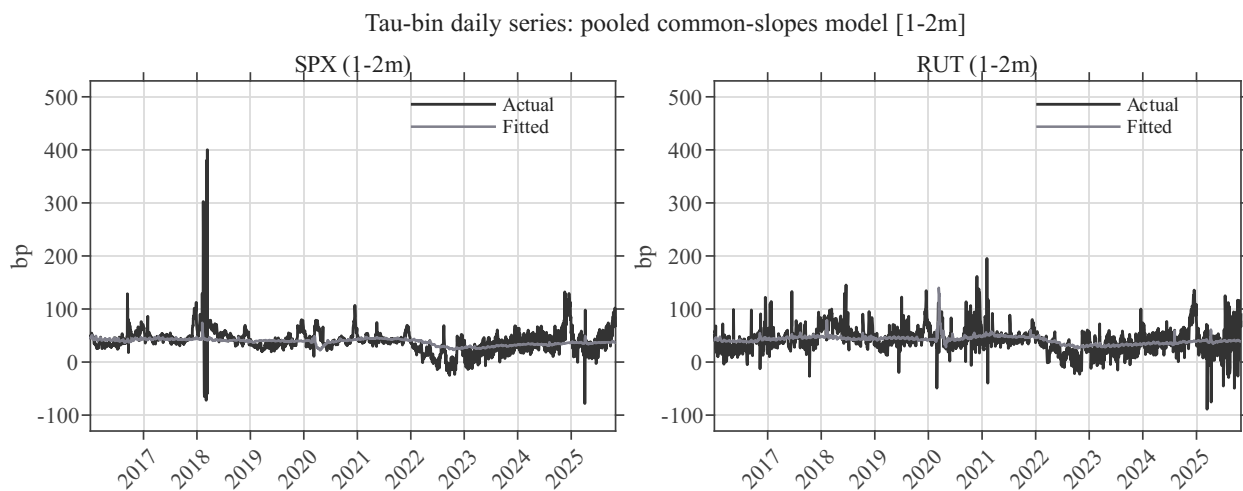


Figure A.1: Time-series fit of the pooled specification: 1–2 month maturity bin.

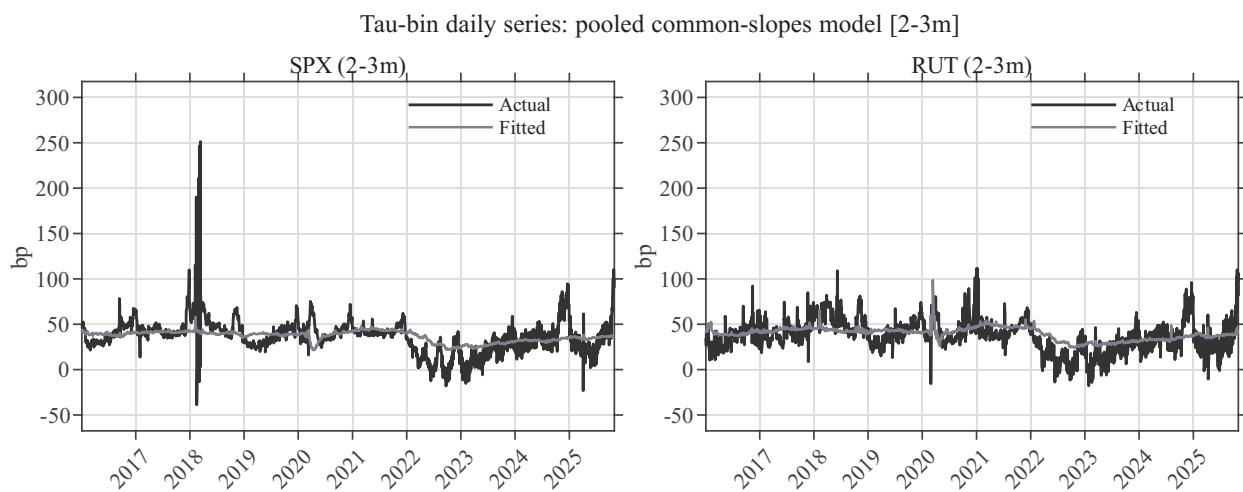


Figure A.2: Time-series fit of the pooled specification: 2–3 month maturity bin.

Tau-bin daily series: pooled common-slopes model [3-5m]

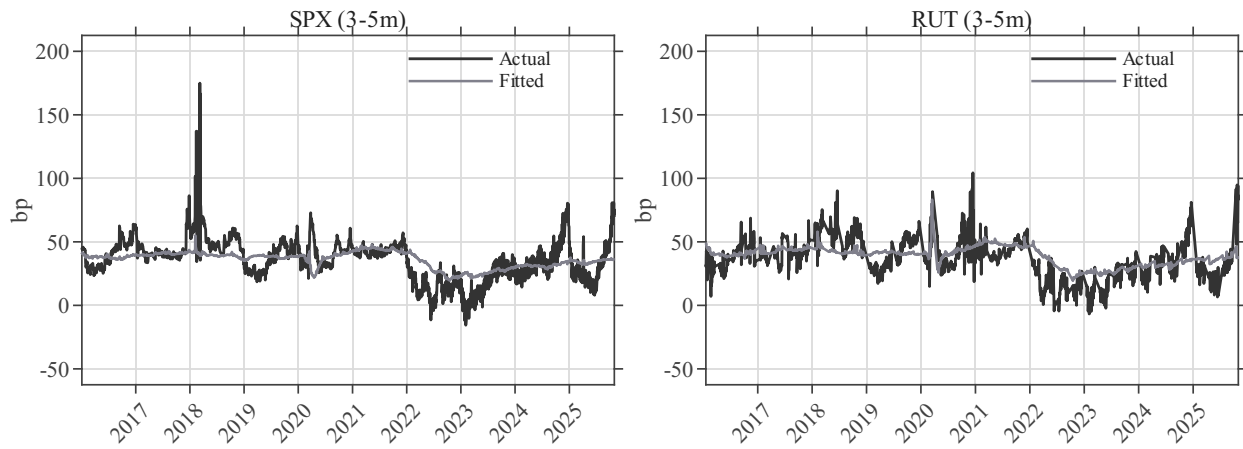


Figure A.3: Time-series fit of the pooled specification: 3–5 month maturity bin.

Tau-bin daily series: pooled common-slopes model [5-7m]

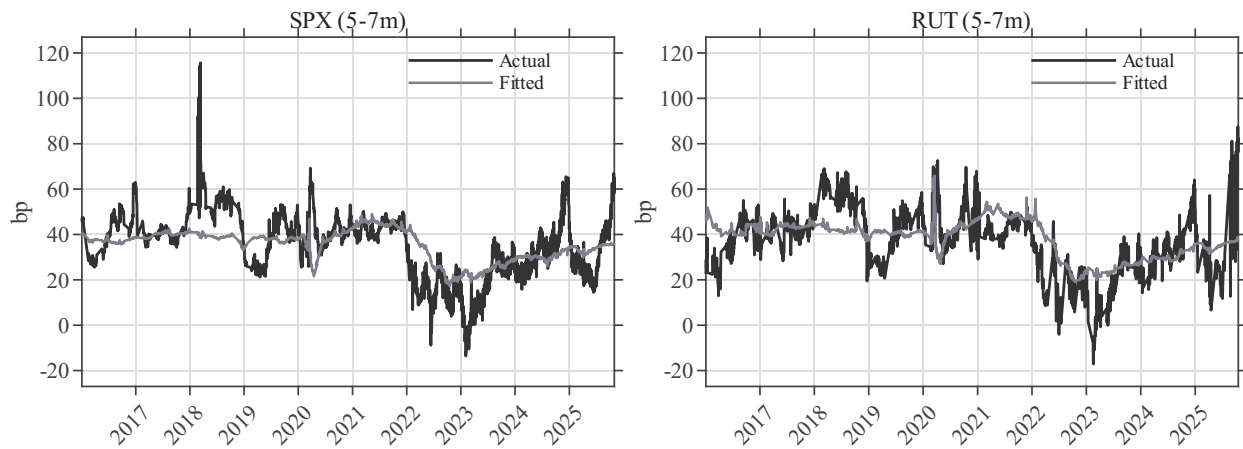


Figure A.4: Time-series fit of the pooled specification: 5–7 month maturity bin.

Tau-bin daily series: pooled common-slopes model [7-10m]

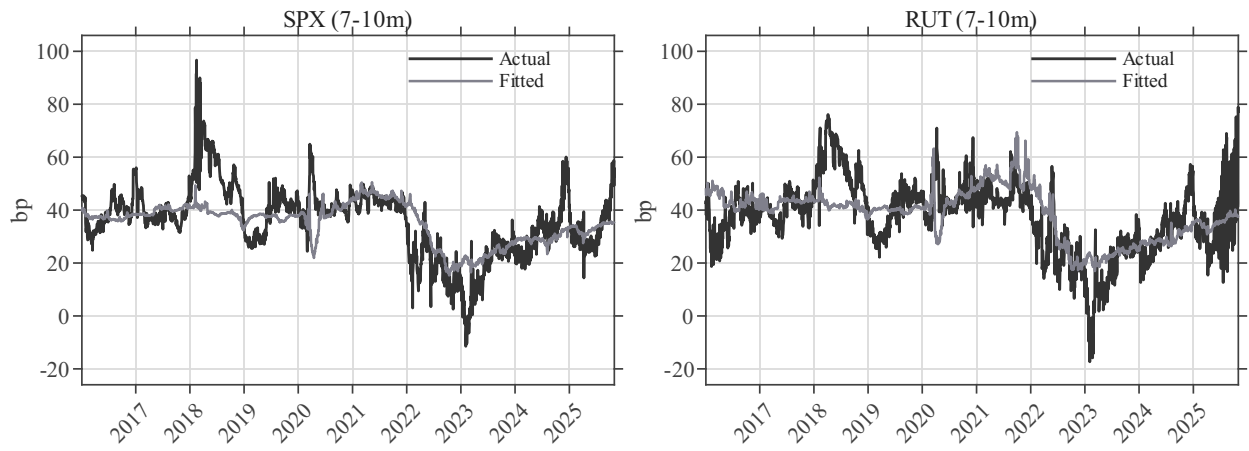


Figure A.5: Time-series fit of the pooled specification: 7–10 month maturity bin.

Tau-bin daily series: pooled common-slopes model [10-14m]

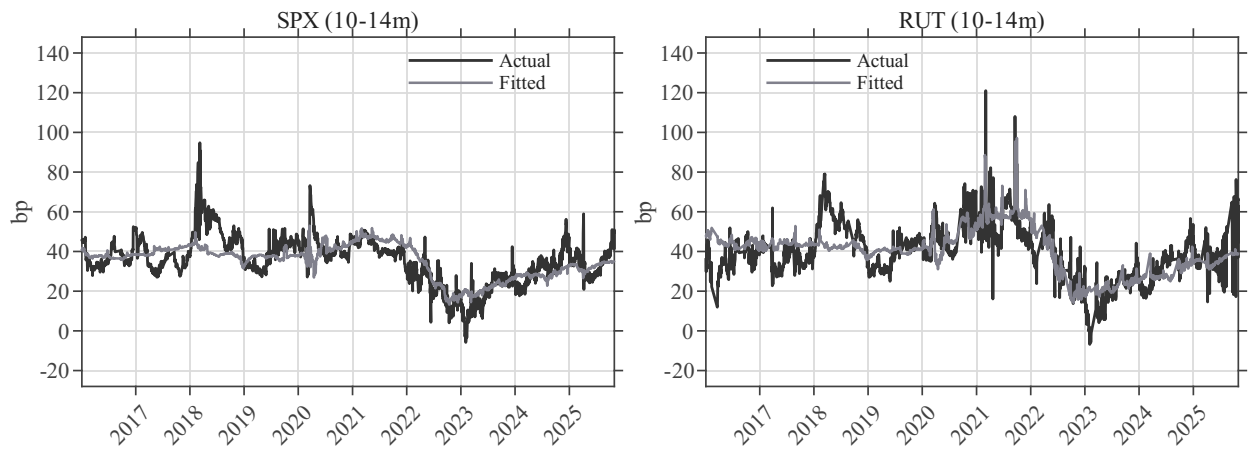


Figure A.6: Time-series fit of the pooled specification: 10–14 month maturity bin.

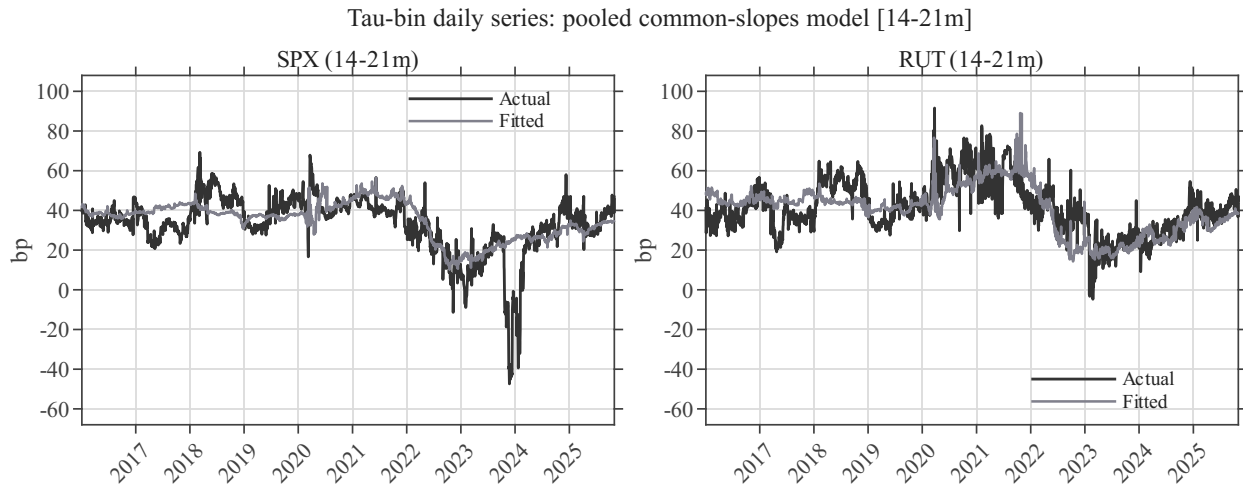


Figure A.7: Time-series fit of the pooled specification: 14–21 month maturity bin.

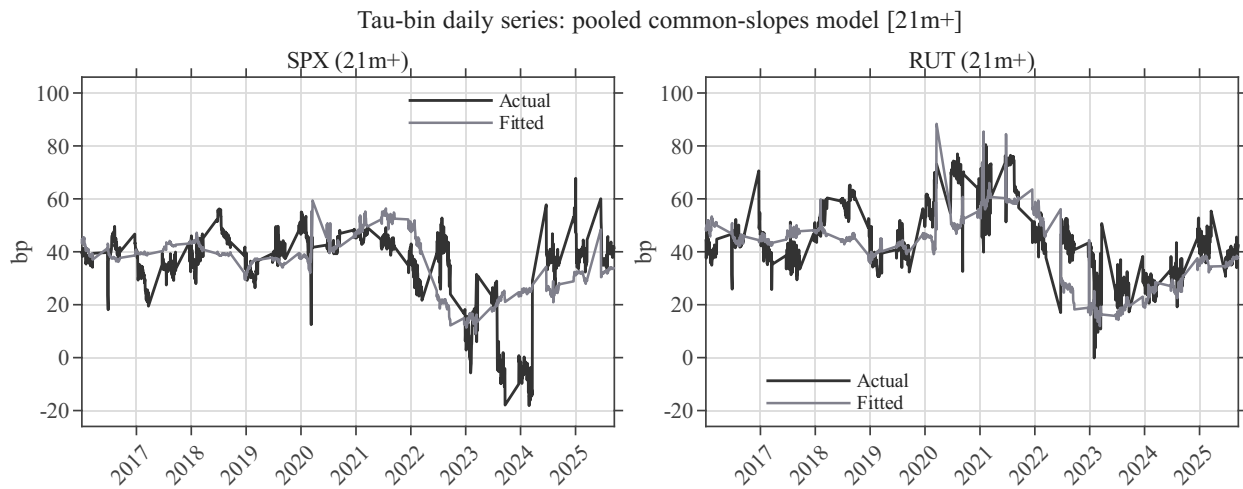


Figure A.8: Time-series fit of the pooled specification: beyond 21 months.

A.2 Separate specifications

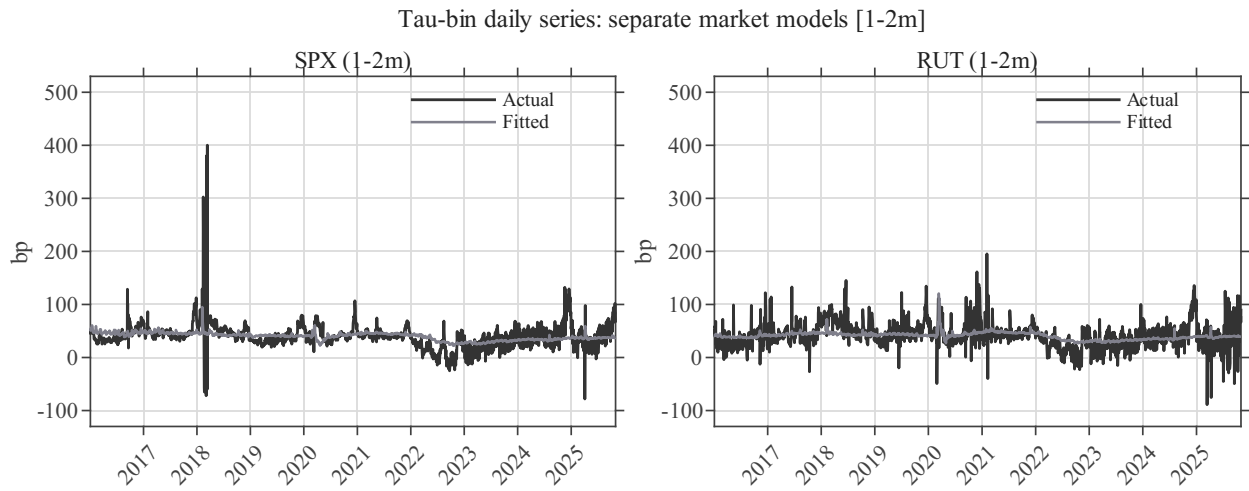


Figure A.9: Time-series fit of the separate specification: 1–2 month maturity bin.

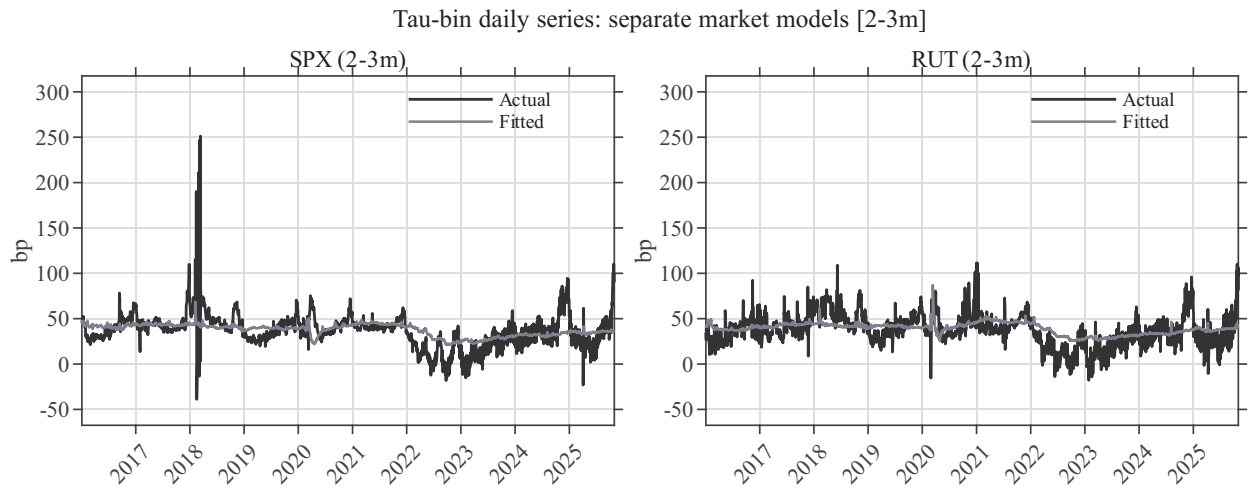


Figure A.10: Time-series fit of the separate specification: 2–3 month maturity bin.

Tau-bin daily series: separate market models [3-5m]

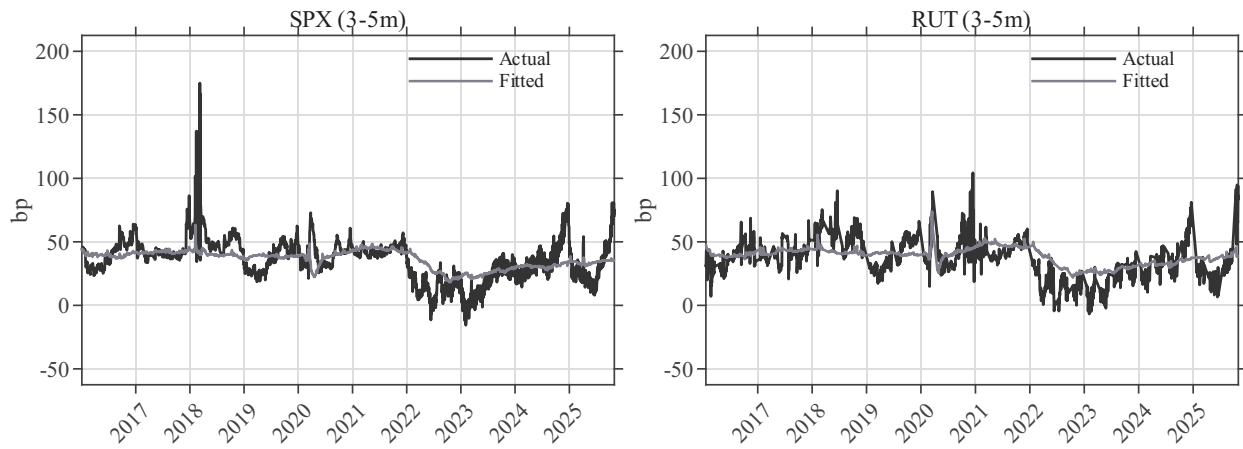


Figure A.11: Time-series fit of the separate specification: 3–5 month maturity bin.

Tau-bin daily series: separate market models [5-7m]

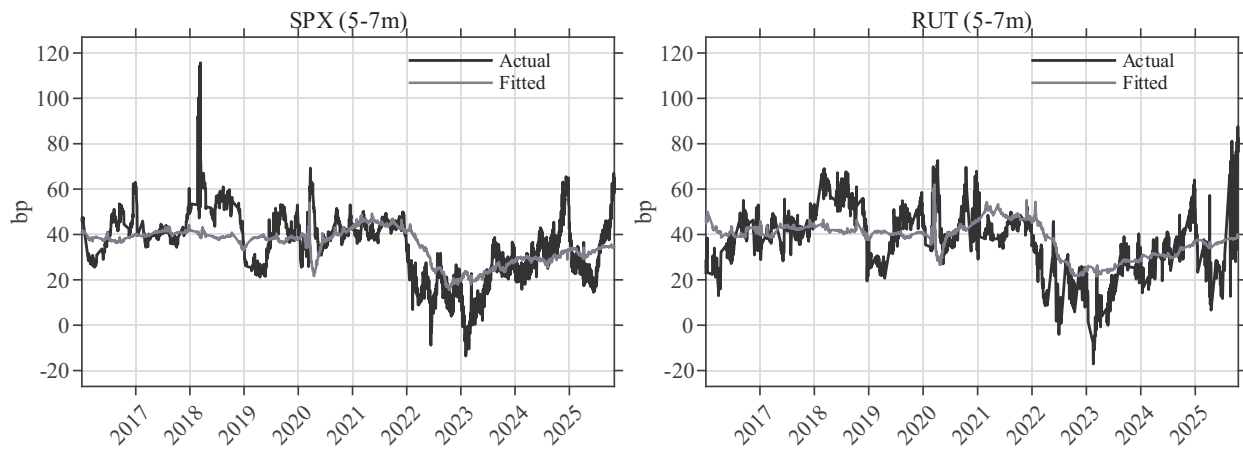


Figure A.12: Time-series fit of the separate specification: 5–7 month maturity bin.

Tau-bin daily series: separate market models [7-10m]

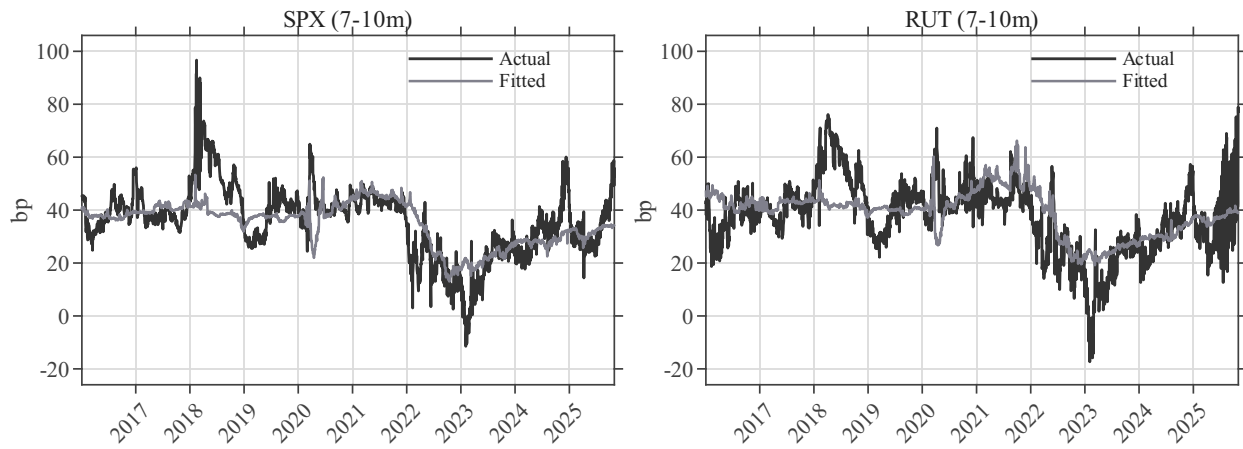


Figure A.13: Time-series fit of the separate specification: 7–10 month maturity bin.

Tau-bin daily series: separate market models [10-14m]

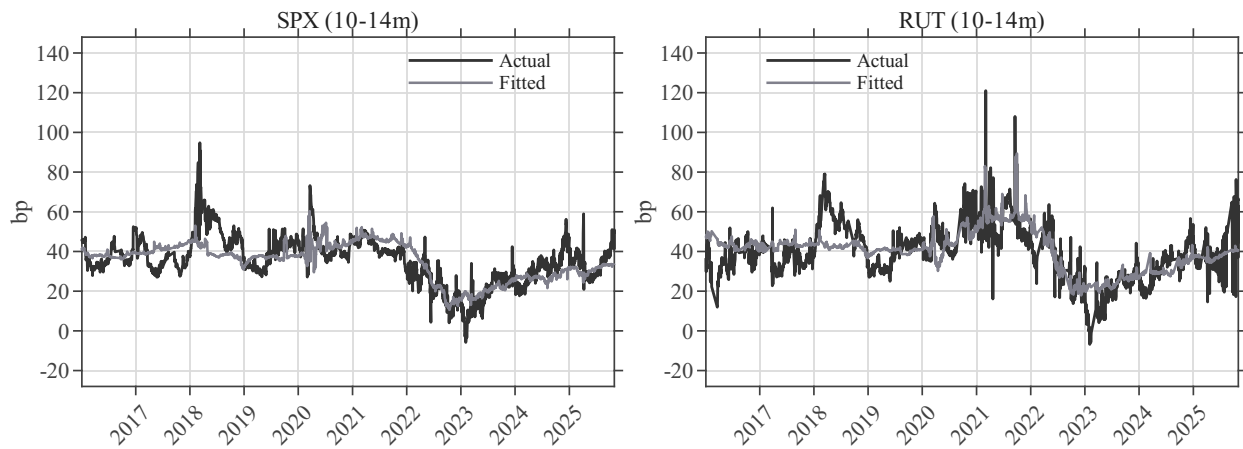


Figure A.14: Time-series fit of the separate specification: 10–14 month maturity bin.

Tau-bin daily series: separate market models [14-21m]

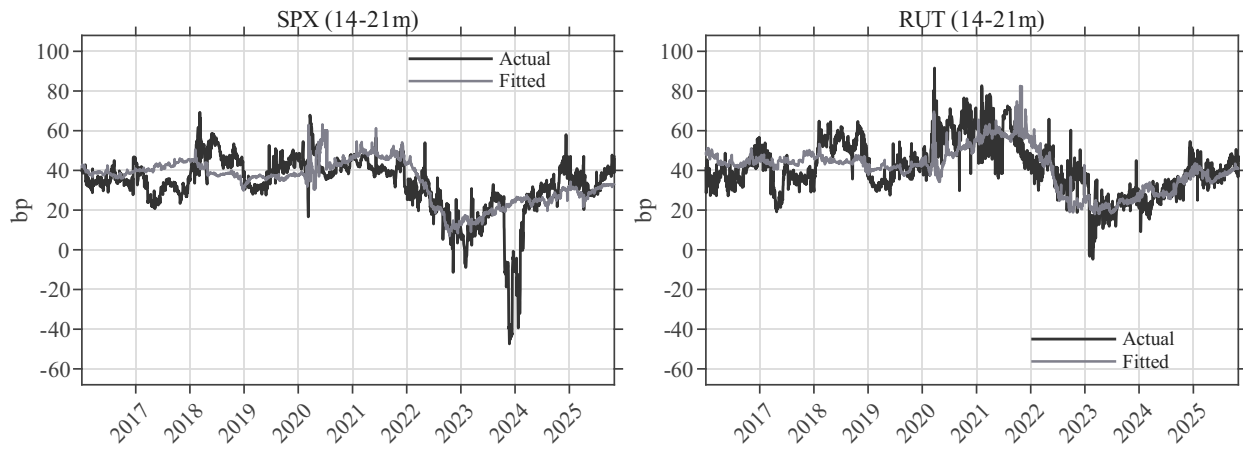


Figure A.15: Time-series fit of the separate specification: 14–21 month maturity bin.

Tau-bin daily series: separate market models [21m+]

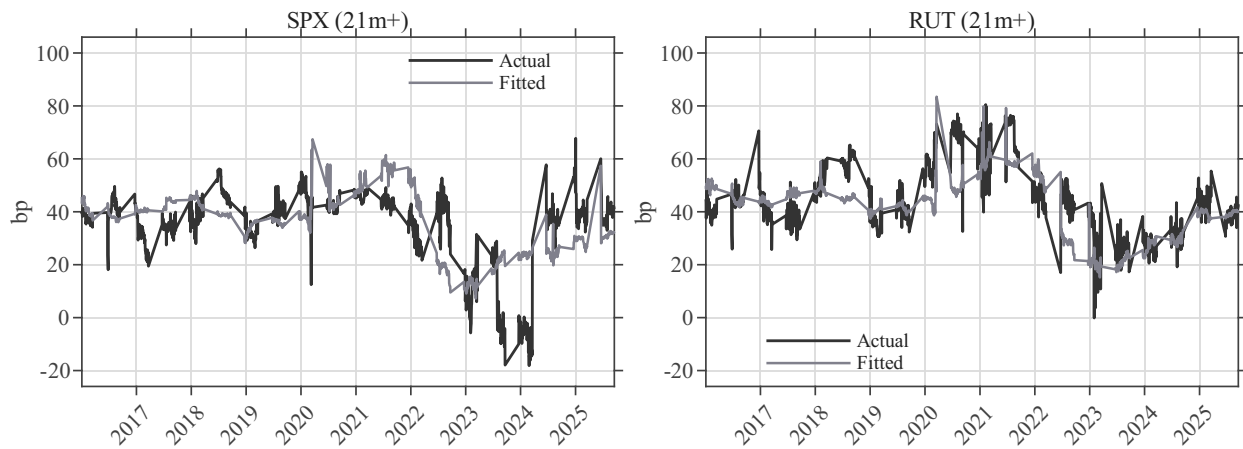


Figure A.16: Time-series fit of the separate specification: beyond 21 months.